
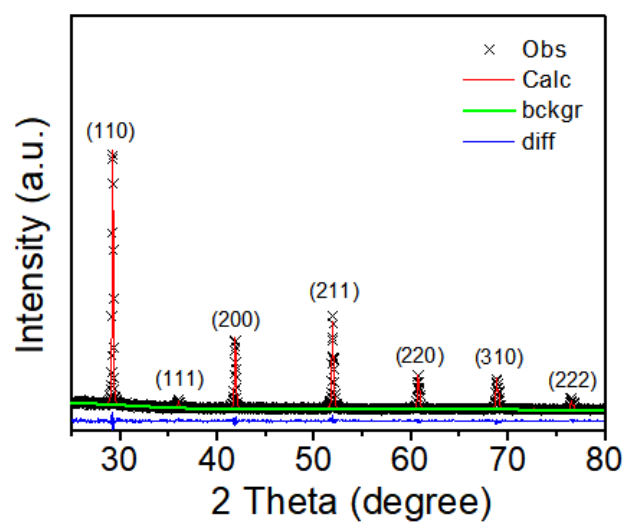


In the format provided by the authors and unedited.

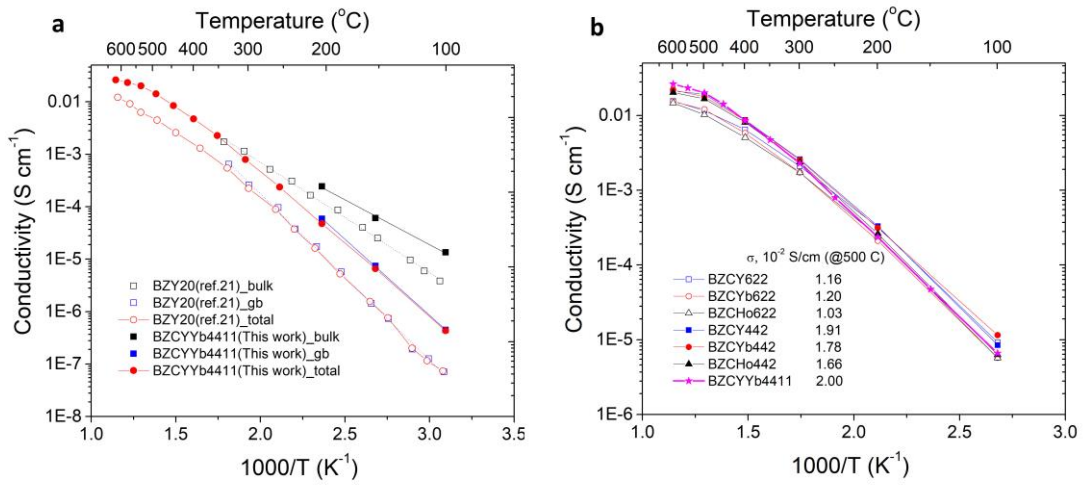
Exceptional power density and stability at intermediate temperatures in protonic ceramic fuel cells

Sihyuk Choi¹, Chris J. Kucharczyk^{1,2}, Yangang Liang³, Xiaohang Zhang³, Ichiro Takeuchi³, Ho-Il Ji^{1,2}  and Sossina M. Haile^{1*}

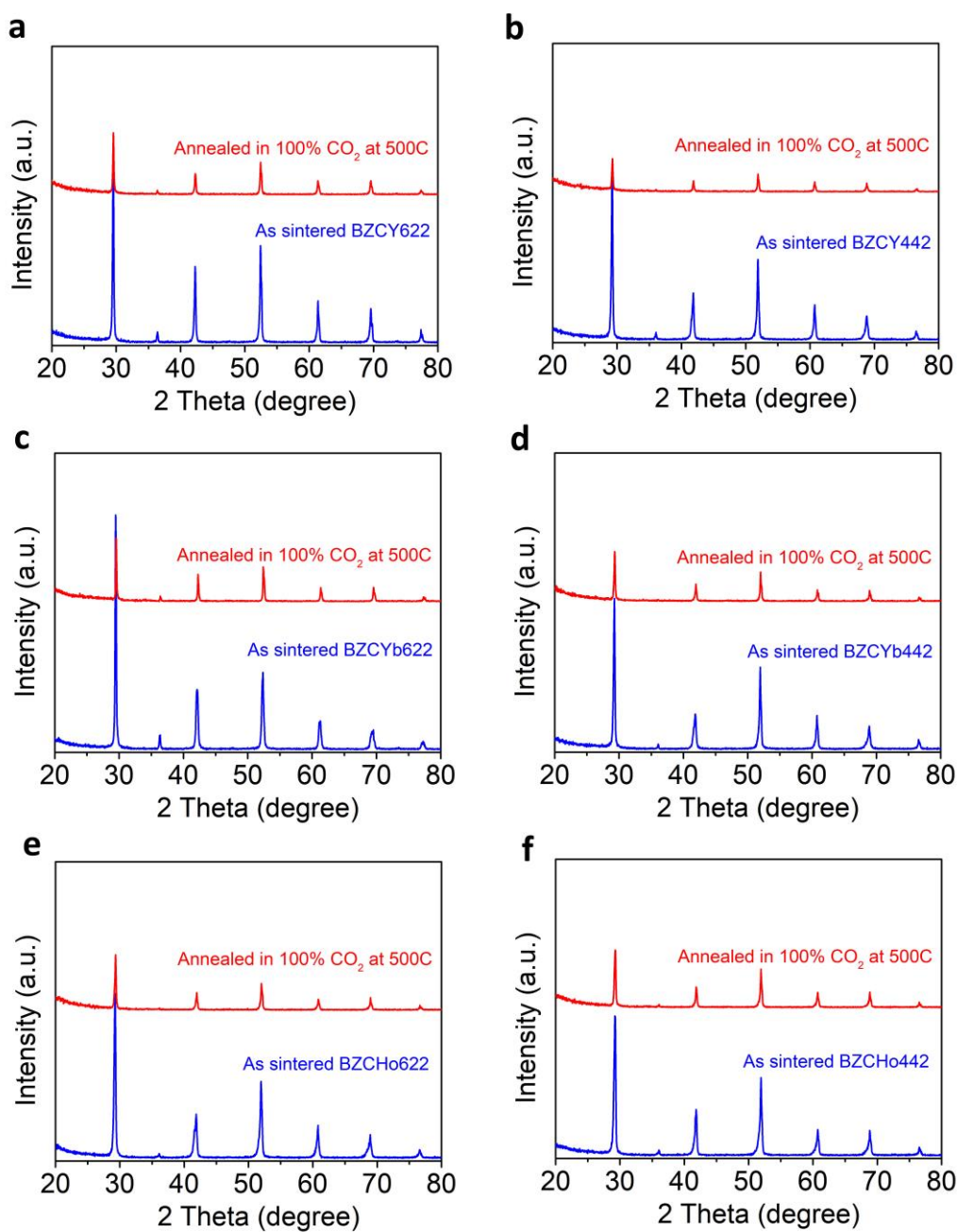
¹Materials Science and Engineering, Northwestern University, Evanston, IL, USA. ²Applied Physics & Materials Science, California Institute of Technology, Pasadena, CA, USA. ³Materials Science and Engineering, University of Maryland, College Park, MD, USA. *e-mail: ssossina.haile@northwestern.edu



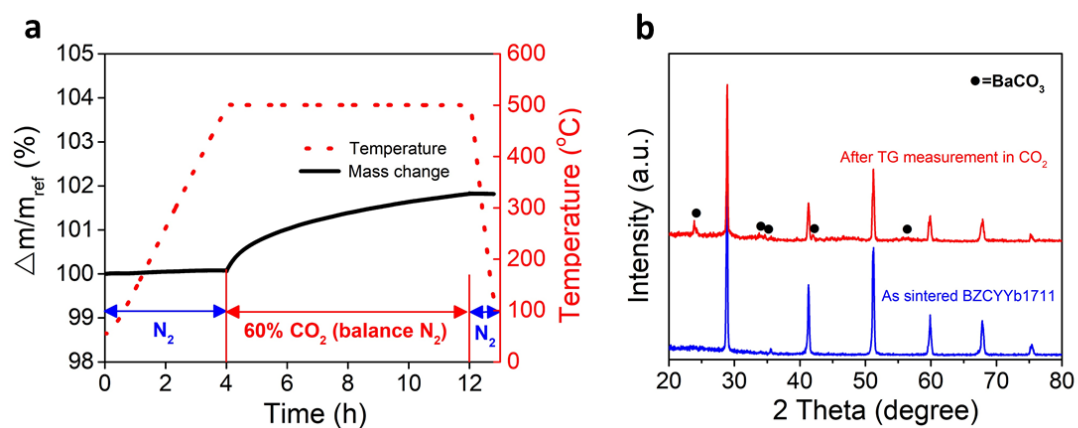
Supplementary Figure 1. Rietveld refinement of the X-ray diffraction pattern for BZCYYb4411 electrolyte. Refinement to a $Pm\bar{3}m$ cubic structure yielded a lattice constant of 4.3060(1) Å. ($R_{wp} = 15.1\%$, $R_p = 9.94\%$, $\chi^2 = 2.249$)



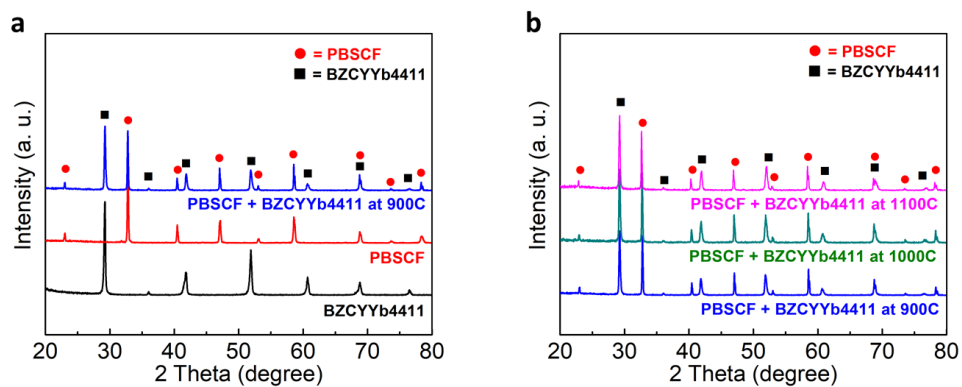
Supplementary Figure 2. Total conductivity comparison of BZCYYb4411 and other proton conducting electrolyte materials. (a) the comparison with BZY20 composition in bulk, grain boundary (gb), and total conductivity. (b) total conductivities of 20 % Y, Yb, and Ho doped barium zirconate-cerate oxide with both 60 % and 40 % Zr concentration.



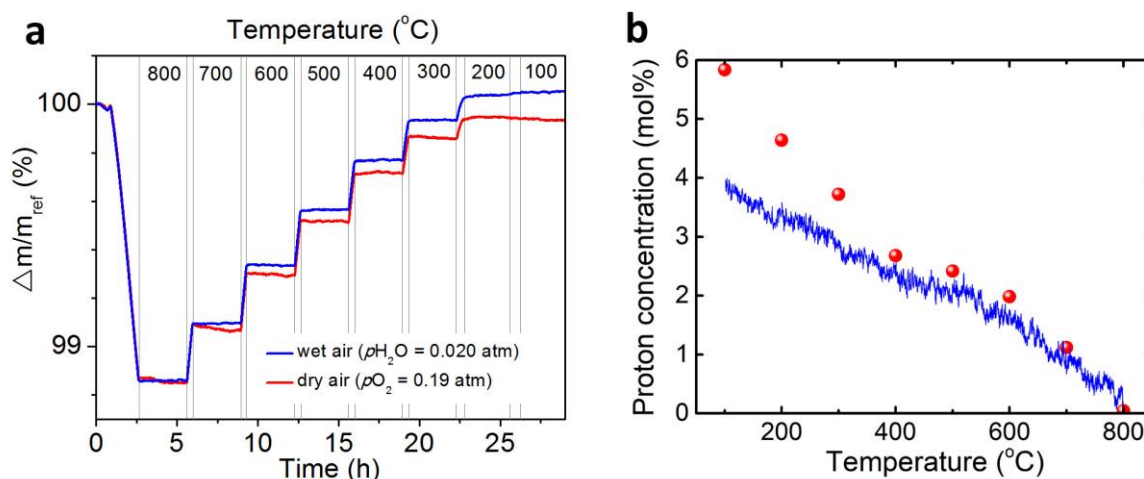
Supplementary Figure 3. Chemical stability of 20% Y, Yb, and Ho doped samples in CO₂. X-ray diffraction patterns of (a) BaZr_{0.6}Ce_{0.2}Y_{0.2}O_{3- δ} (BZCY622), (b) BaZr_{0.4}Ce_{0.4}Y_{0.2}O_{3- δ} (BZCY442), (c) BaZr_{0.6}Ce_{0.2}Yb_{0.2}O_{3- δ} (BZCYb622), (d) BaZr_{0.4}Ce_{0.4}Yb_{0.2}O_{3- δ} (BZCYb442), (e) BaZr_{0.6}Ce_{0.2}Ho_{0.2}O_{3- δ} (BZCHo622), and (f) BaZr_{0.4}Ce_{0.4}Ho_{0.2}O_{3- δ} (BZCHo442) collected in the as-sintered state and after exposure to 100 % CO₂ at 500 °C for 12h.



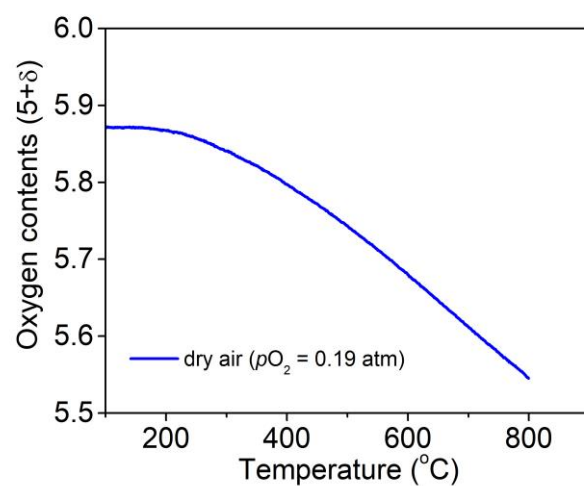
Supplementary Figure 4. Chemical stability of BZCYYb1711 in CO_2 . (a) Thermogravimetric profile for exposure of BZCYYb1711 powder to 60 % CO_2 (balance N_2) at 600 $^{\circ}\text{C}$. The observed weight gain of BZCYYb1711 reflects reaction with CO_2 to form carbonates. (b) X-ray diffraction patterns of BZCYYb1711 before and after thermogravimetric analysis in CO_2 -containing atmospheres showing secondary peaks corresponding to barium carbonate.



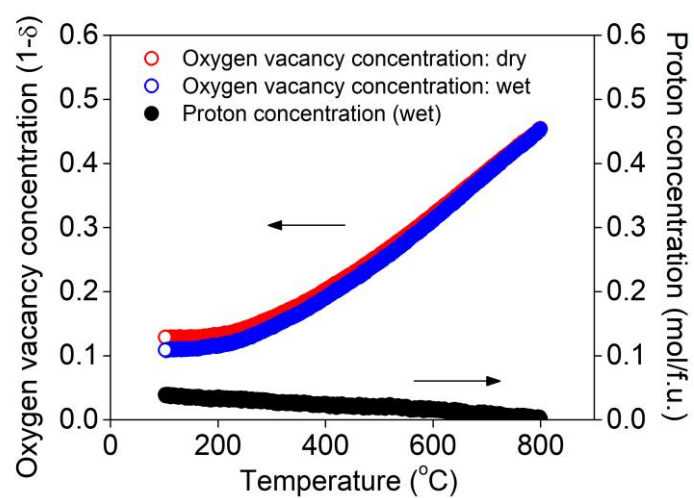
Supplementary Figure 5. Chemical compatibility between PBSCF cathode and BZCYYb electrolyte. (a) X-ray diffraction patterns for sintered BZCYYb4411 and PBSCF pellets are shown as references for the diffraction pattern of a mixture of the two materials annealed at 900 °C. No secondary peaks occur, indicating the absence of a reaction between these phases. (b) X-ray diffraction patterns for the mixture annealed at 900, 1000, and 1100 °C also show no secondary phases.



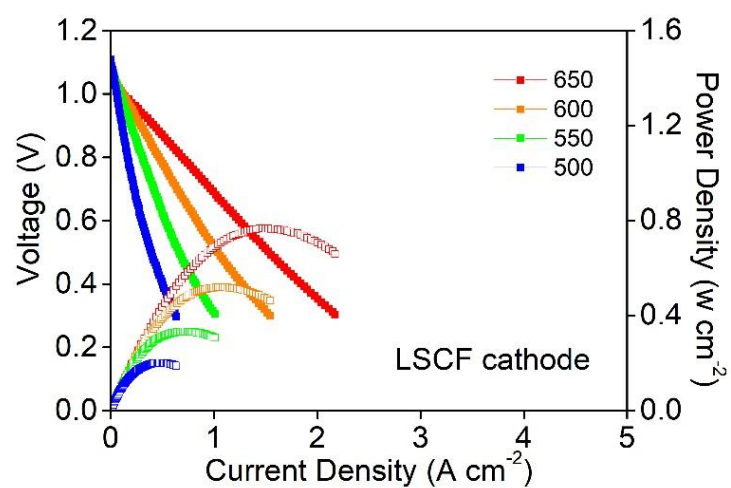
Supplementary Figure 6. (a) Thermogravimetric profiles on step-wise cooling in dry and wet air; and (b) comparison of proton concentrations obtained from continuous (0.5 °C min^{-1}) and step-wise (increments of 100 °C and 3 h hold) cooling. Moderate disagreement at low temperature is tentatively assigned to surface hydration effects, which are sensitive to differences in specific surface area (and are not of relevance to understanding bulk hydration behavior). A van't Hoff analysis of the data collected under step-wise cooling over the range 200 to 600 °C, yields enthalpy and entropy values of -23 ± 2 kJ mol^{-1} and -63 ± 3 J mol^{-1} K^{-1} , respectively, identical to the values at 400 °C obtained from the analysis of the data collected under continuous cooling.



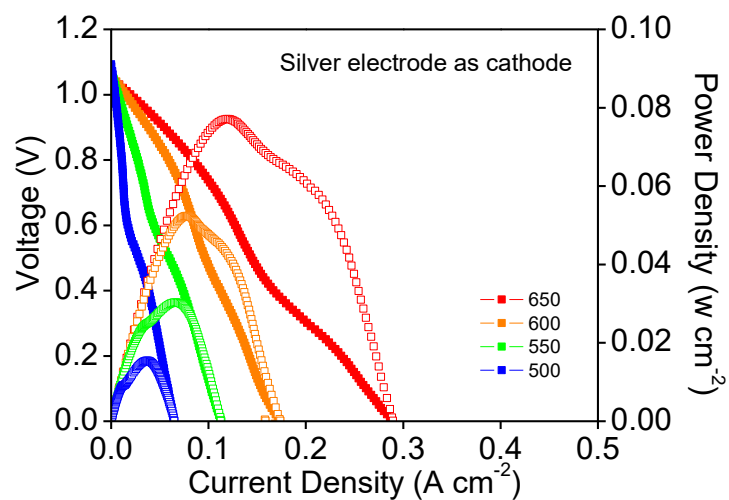
Supplementary Figure 7. Temperature dependence of oxygen concentration in PBSCF in dry air. Oxygen non-stoichiometry data for PBSCF in dry air as determined by thermogravimetric analysis. Initial oxygen content is 5.88 at 100 °C (ref. 30).



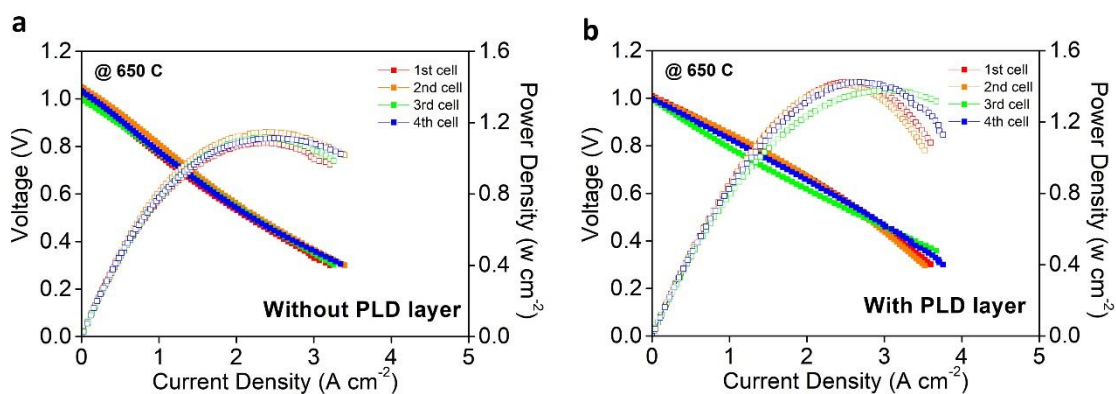
Supplementary Figure 8. PBSCF defect concentrations as a function of temperature under both dry and wet conditions, as determined from thermogravimetric analysis. Concentrations are given in units of moles of species per mole of double-perovskite formula unit.



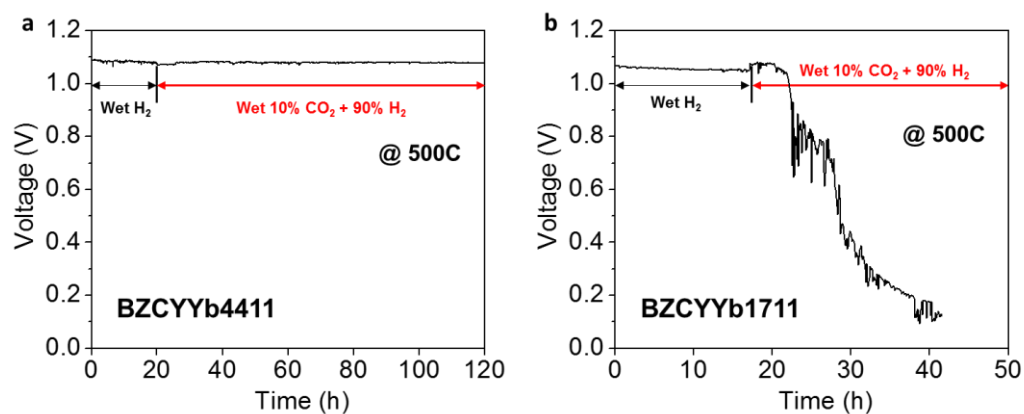
Supplementary Figure 9. *IV* curves and corresponding power densities of a BZCYYb4411-based cell with LSCF as the cathode. The peak power densities at 600 and 500 °C are only 519 and 201 mW cm⁻², respectively.



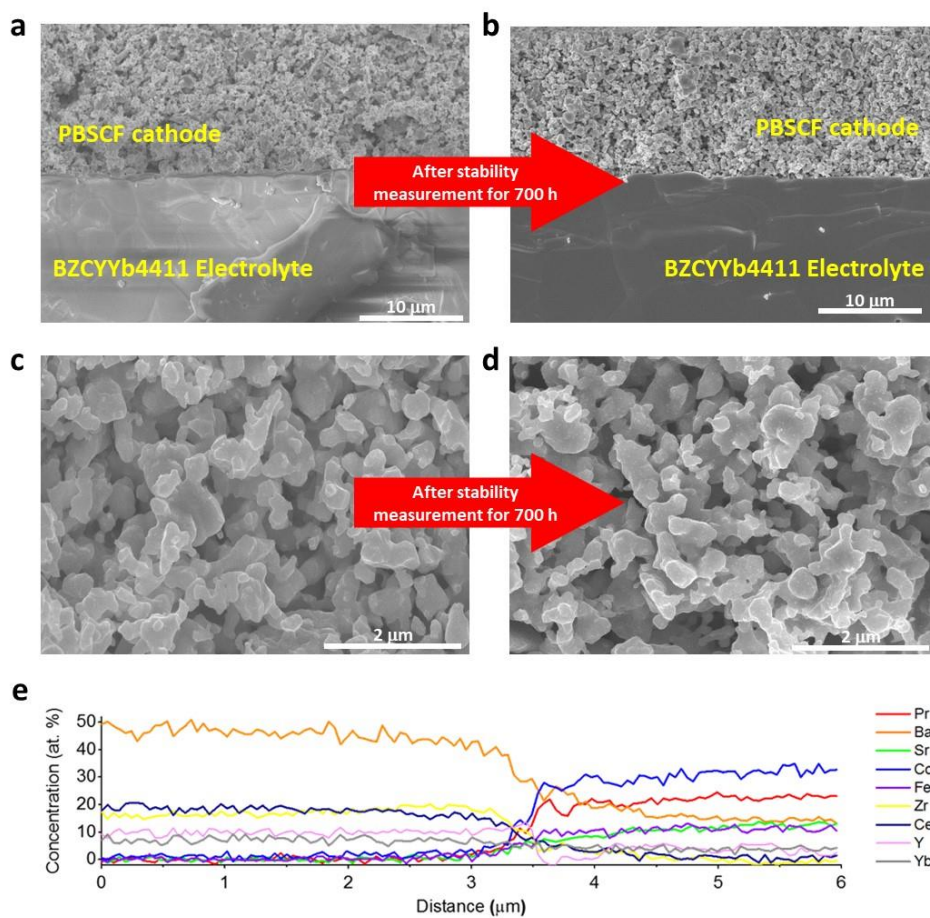
Supplementary Figure 10. *IV* curves and corresponding power densities of a BZCYYb4411-based cell in which silver alone as the cathode. As with all other cells examined, the configuration is an anode-supported thin electrolyte cell with Ni+BZCYYb4411 as the anode. The peak power density when silver alone serves as the cathode is more than 15 times lower than that of analogous cells with a PBSCF cathode.



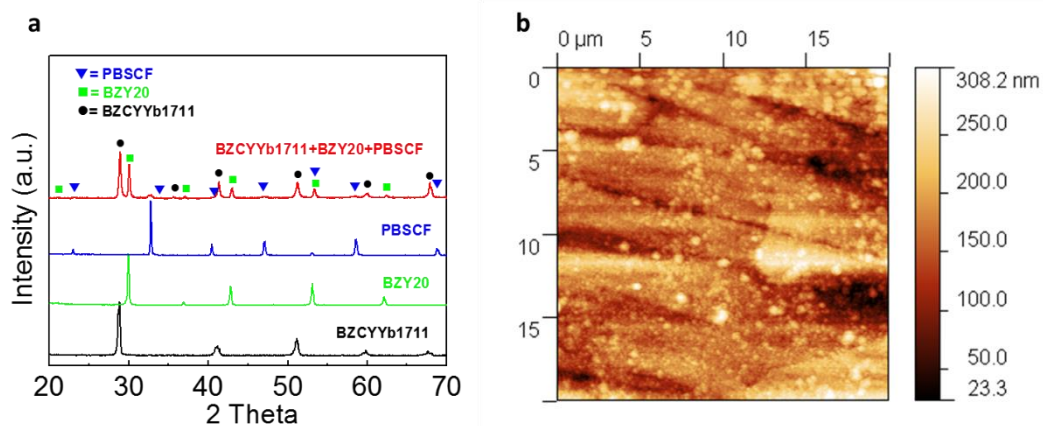
Supplementary Figure 11. *IV* curves and corresponding power densities of BZCYYb4411-based cells at 650 °C. As with all other cells examined, the configuration is an anode-supported thin electrolyte cell with Ni+BZCYYb4411 as the anode, air is supplied to the cathode and humidified hydrogen to the anode. (a) cells without a PLD layer and (b) with a PLD layer. In both cases, curves noted as 1st and 2nd cell are from samples used to obtain results in the main text shown in Figure 4.



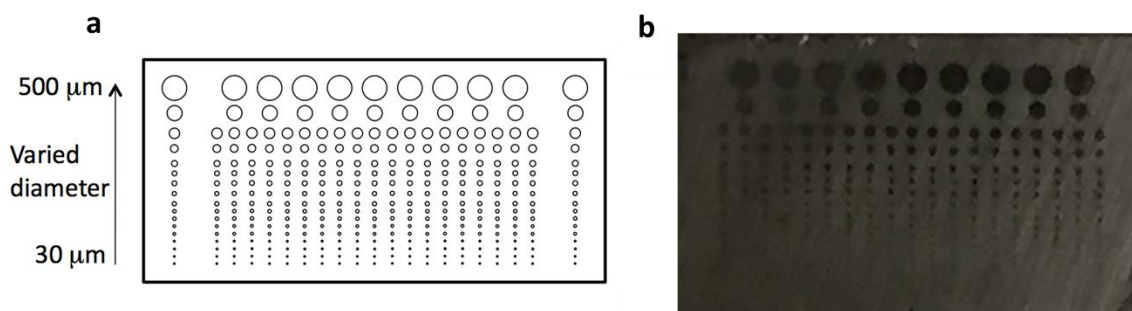
Supplementary Figure 12. Temporal evolution of fuel cell OCV at 500 °C with humidified (3% H₂O) 10% CO₂ and 90% H₂ supplied to the anode and air to the cathode using cells of two different electrolytes: (a) BZCYYb4411 and (b) BZCYYb1711. The OCV from the BZCYYb4411-based cell is extremely stable for a 100 h period of measurement, deviating from the initial value by no more than 1 %. In contrast, the OCV of the BZCYYb1711-based falls by 86% OCV in just 20 h, clearly reflecting the chemical instability of BZCYYb1711.



Supplementary Figure 13. Scanning electron microscopy images before and after stability measurement for 700 h. Interface between PBSCF cathode and BZCYb4411 electrolyte (a) before stability measurement. (b) after stability measurement. High-magnification of microstructure of cathode. (c) before stability measurement. (d) after stability measurement. (e) EDS line scan at the cathode and electrolyte interface after stability measurement.



Supplementary Figure 14. Characterization of PBSCF microdot electrodes. (a) Diffraction patterns for BZCYYb1711 (substrate), BZY20 (buffer layer), and PBSCF cathode. (b) Atomic force micrographs of microdot electrode with a root-mean-squared roughness of 43.8 nm.



Supplementary Figure 15. Layout of a library of PBSCF thin film microelectrodes. (a) Schematic image showing microdots varying in diameter from 30 μm to 500 μm with roughly logarithmic spacing. (b) Optical microscope image.

Supplementary Table 1. PCFCs for which peak power density approaches or exceeds 90 mWcm⁻² at 500 °C with air supplied to the cathode and humidified hydrogen to the anode. PPD = peak power density; OCV = open circuit voltage; R_o = area-specific ohmic resistance (measured / expected based on electrolyte thickness, assuming a conductivity at 500 °C of $1.5 \times 10^{-2} \Omega^{-1}\text{cm}^{-1}$ for all electrolyte compositions); R_p = area-specific polarization resistance.

Electrolyte	Anode	Cathode	PPD (mWcm ⁻²)	OCV (V)	R_o (Ωcm^2)	R_p (Ωcm^2)	Source
100 nm BZY20	Pt	Pt	>140 ^a	1.05	n/a / 6.7×10^{-2}	n/a	Shim, 2009 (1)
35 μm BaZr4Ce4Y2	Ni + elyte	Ba _{0.5} Sr _{0.5} Co _{0.8} Fe _{0.2} O _{3-δ}	115	1.07	1.5/0.23	0.4	Guo, 2009 (2)
20 μm BZY10	Ni-BZY20	PrBaCo ₂ O _{5+δ} + BZPY10	92	1.01	1.53/0.13	1.18	Bi, 2011 (3)
20 μm BaZr1Ce7Y2	Ni + elyte	Ba _{0.5} Sr _{0.5} FeO _{3-δ} + SDC	95	1.08	0.6/0.13	3.7	Sun, 2010 (4)
15 μm BaZr1Ce7Y1Yb1	Ni + elyte	Ba _{0.5} Sr _{0.5} Fe _{0.8} Cu _{0.2} O _{3-δ} + SDC	121	1.07	0.58/0.10	2.62	Ling, 2011 (5)
12 μm BaZr1Ce7Y2	Ni + elyte	La _{0.7} Sr _{0.3} FeO _{3-δ} + SDC	175	1.09	0.76/0.080	1.5	Sun, 2011 (6)
18 μm BaZr1Ce7Y2	Ni + elyte	SSC (dry O ₂ as oxidant)	587	1.12	0.45/0.12	0.2	Nien, 2011 (7)
40 μm BaZr1Ce7Y2	Ni + elyte ^b	BaCo _{0.7} Fe _{0.2} Nd _{0.1} O _{3-δ}	130	1.07	n/a / 0.27	1.8	Lin, 2012 (8)
20 μm BaZr4Ce4Y2	Ni + elyte	BSCFT + elyte	95	1.07	1.4/0.13	1.7	Bi, 2012 (9)
20 μm BaZr1Ce7Y2	Ni + elyte	GBSC + elyte	120	1.07	0.75/0.13	1.6	Zhang, 2013 (10)
10 μm BaZr1Ce7Y1Yb1	Ni + elyte	LSCF	230	1.12	0.24/0.067	0.71	Nguyen, 2013 (11)
15 μm BaZr1Ce7Y1Yb1	Ni + elyte	NBSCF	~150 ^c	N/A	0.24 [§] /0.10	1.4 [§]	Kim, 2014 (12)
~25 μm BaZr1Ce7Y1Yb1+NiO	Ni + elyte	BaCo _{0.4} Fe _{0.4} Zr _{0.1} Y _{0.1} O _{3-δ}	455	1.13	n/a / 0.17	n/a	Duan, 2015 (13)
~25 μm BaZr3Ce6Y1 + CuO	Ni + elyte	BaCo _{0.4} Fe _{0.4} Zr _{0.1} Y _{0.1} O _{3-δ}	318		n/a / 0.17	n/a	Duan, 2015
~25 μm BZY + NiO	Ni + elyte	BaCo _{0.4} Fe _{0.4} Zr _{0.1} Y _{0.1} O _{3-δ}	335		n/a / 0.17	n/a	Duan, 2015
~2.5 μm BZY15 (PLD)	Ni + elyte	La _{0.6} Sr _{0.4} CoO _{3-δ}	457	1.0	0.15/0.017	0.75	Bae, 2017 (14)
15 μm 4411 (w/PLD)_1 st cell	Ni + elyte	PBSCF	528	1.12	0.18/0.10	0.55	this work
15 μm 4411 (w/PLD)_2 nd cell	Ni + elyte	PBSCF	548	1.09	0.15/0.10	0.58	this work
15 μm 4411 (no PLD)_1 st cell	Ni + elyte	PBSCF	377	1.05	0.29/0.10	0.74	this work
15 μm 4411 (no PLD)_2 nd cell	Ni + elyte	PBSCF	416	1.14	0.27/0.10	0.76	this work
15 μm 4411	Ni + elyte	LSCF	201	1.10	0.41/0.10	2.07	this work

BZY20 = BaZr_{0.8}Y_{0.2}O_{3- δ} ; BZY10 = BaZr_{0.9}Y_{0.1}O_{3- δ} ; BaZr4Ce4Y2 = BaZr_{0.4}Ce_{0.4}Y_{0.2}O_{3- δ} ; BZPY10 = BaZr_{0.4}Ce_{0.4}Y_{0.2}O_{3- δ} ; BaZr1Ce7Y1Yb1 = BaZr_{0.1}Ce_{0.7}Y_{0.1}Yb_{0.1}O_{3- δ} ; BaZr1Ce7Y2 = BaZr_{0.1}Ce_{0.7}Y_{0.2}O_{3- δ} ; SDC = samaria doped ceria (15-20 at%); SSC = Sm_{0.5}Sr_{0.5}CoO₃; BSCFT = Ba_{0.5}Sr_{0.5}(Co_{0.8}Fe_{0.2})_{0.9}Ti_{0.1}O_{3- δ} ; GBSC = GdBa_{0.5}Sr_{0.5}Co₂O_{5+ δ} ; LSCF = (La,Sr)(Co,Fe)O₃, precise composition not specified; NBSCF = NdBa_{0.5}Sr_{0.5}Co_{1.5}FeO_{5+ δ} ; PBSCF = PrBa_{0.5}Sr_{0.5}Co_{1.5}FeO_{5+ δ} ; elyte = electrolyte; n/a = not available

^a amorphous film, results at 400 °C, current not sufficiently high to reach peak power density.

^b material not reported, but is likely such a composite.

^c extrapolated from measurements between 750 and 600 °C.

Supplementary References

- 1 Shim, J. H. *et al.* Intermediate-Temperature Ceramic Fuel Cells with Thin Film Yttrium Doped Barium Zirconate Electrolytes. *Chem. Mater.* **21**, 3290-3296 (2009).
- 2 Guo, Y., Lin, Y., Ran, R. & Shao, Z. Zirconium doping effect on the performance of proton-conducting $\text{BaZr}_y\text{Ce}_{0.8-y}\text{Y}_{0.2}\text{O}_{3-\delta}$ ($0.0 \leq y \leq 0.8$) for fuel cell applications. *J. Power Sources* **193**, 400-407 (2009).
- 3 Bi, L., Fabbri, E., Sun, Z. & Traversa, E. A novel ionic diffusion strategy to fabricate high-performance anode-supported solid oxide fuel cells (SOFCs) with proton-conducting Y-doped BaZrO_3 films. *Energy Environ. Sci.* **4**, 409-412, (2011).
- 4 Sun, W. *et al.* A high performance $\text{BaZr}_{0.1}\text{Ce}_{0.7}\text{Y}_{0.2}\text{O}_{3-\delta}$ -based solid oxide fuel cell with a cobalt-free $\text{Ba}_{0.5}\text{Sr}_{0.5}\text{FeO}_{3-\delta}$ - $\text{Ce}_{0.8}\text{Sm}_{0.2}\text{O}_{2-\delta}$ composite cathode. *Int. J. Hydrogen Energy* **35**, 7925-7929 (2010).
- 5 Ling, Y., Yu, J., Zhang, X., Zhao, L. & Liu, X. A cobalt-free $\text{Sm}_{0.5}\text{Sr}_{0.5}\text{Fe}_{0.8}\text{Cu}_{0.2}\text{O}_{3-\delta}$ - $\text{Ce}_{0.8}\text{Sm}_{0.2}\text{O}_{2-\delta}$ composite cathode for proton-conducting solid oxide fuel cells. *J. Power Sources* **196**, 2631-2634 (2011).
- 6 Sun, W. *et al.* Optimization of $\text{BaZr}_{0.1}\text{Ce}_{0.7}\text{Y}_{0.2}\text{O}_{3-\delta}$ -based proton-conducting solid oxide fuel cells with a cobalt-free proton-blocking $\text{La}_{0.7}\text{Sr}_{0.3}\text{FeO}_{3-\delta}$ - $\text{Ce}_{0.8}\text{Sm}_{0.2}\text{O}_{2-\delta}$ composite cathode. *Int. J. Hydrogen Energy* **36**, 9956-9966 (2011).
- 7 Nien, S. H., Hsu, C. S., Chang, C. L. & Hwang, B. H. Preparation of $\text{BaZr}_{0.1}\text{Ce}_{0.7}\text{Y}_{0.2}\text{O}_{3-\delta}$ Based Solid Oxide Fuel Cells with Anode Functional Layers by Tape Casting. *Fuel Cells* **11**, 178-183 (2011).
- 8 Lin, Y., Zhou, W., Sunarso, J., Ran, R. & Shao, Z. Characterization and evaluation of $\text{BaCo}_{0.7}\text{Fe}_{0.2}\text{Nb}_{0.1}\text{O}_{3-\delta}$ as a cathode for proton-conducting solid oxide fuel cells. *Int. J. Hydrogen Energy* **37**, 484-497 (2012).
- 9 Bi, L., Fabbri, E. & Traversa, E. Effect of anode functional layer on the performance of proton-conducting solid oxide fuel cells (SOFCs). *Electrochem. Commun.* **16**, 37-40 (2012).
- 10 Zhang, X. *et al.* A highly active anode functional layer for solid oxide fuel cells based on proton-conducting electrolyte $\text{BaZr}_{0.1}\text{Ce}_{0.7}\text{Y}_{0.2}\text{O}_{3-\delta}$. *J. Power Sources* **241**, 654-659 (2013).
- 11 Nguyen, N. T. Q. & Yoon, H. H. Preparation and evaluation of $\text{BaZr}_{0.1}\text{Ce}_{0.7}\text{Y}_{0.1}\text{Yb}_{0.1}\text{O}_{3-\delta}$ (BZCYYb) electrolyte and BZCYYb-based solid oxide fuel cells. *J. Power Sources* **231**, 213-218 (2013).

- 12 Kim, J. *et al.* Triple-Conducting Layered Perovskites as Cathode Materials for Proton-Conducting Solid Oxide Fuel Cells. *ChemSusChem* **7**, 2811-2815 (2014).
- 13 Duan, C. *et al.* Readily processed protonic ceramic fuel cells with high performance at low temperatures. *Science* **349**, 1321-1326 (2015).
- 14 Bae, K. *et al.* Demonstrating the potential of yttrium-doped barium zirconate electrolyte for high-performance fuel cells. *Nat. Commun.* **8**, 14553 (2017).